

## Supporting Information

### **N-doped carbon coating enhance bifunctional oxygen reaction activity of CoFe nanoparticles for high stable Zn-air battery**

*Qi Liu,<sup>a,b</sup> Xu Liu,<sup>a</sup> Ying Xie,<sup>a</sup> Fanfei Sun,<sup>c</sup> Zhijian Liang,<sup>a</sup> Lei Wang,<sup>\*a</sup> and Honggang Fu<sup>\*a</sup>*

<sup>a</sup> Key Laboratory of Functional Inorganic Material Chemistry, Ministry of Education of the People's Republic of China, Heilongjiang University, Harbin 150080, China.  
E-mail: wanglei0525@hlju.edu.cn; fuhg@vip.sina.com; fuhg@hlju.edu.cn.

<sup>b</sup> Key Laboratory of Superlight Materials and Surface Technology of Ministry of Education of the People's Republic of China, Harbin Engineering University, Harbin 150001, China.

<sup>c</sup> Shanghai Synchrotron Radiation Facility, Shanghai Institute of Applied Physics, Chinese Academy of Sciences, Shanghai 201204, China.

## Table of Contents:

1. **Fig. S1** Contact angle photos of CC before (a) and after (b) oxidation treatment.
2. **Fig. S2** SEM images of CC before (a, b) and after (c, d) oxidation treatment.
3. **Fig. S3** (a) TEM and (b,c) HRTEM images of CoFe LDH/CC sample.
4. **Fig. S4** SEM images of CoFe LDH grown on carbon cloth without oxidation treatment.
5. **Fig. S5** SEM images of (a) CoFe LDH-30 and (b) CoFe LDH-150 samples.
6. **Fig. S6** SEM images of (a, b) CoFe LDH@PPy/CC-5 (electrochemical polymerization of pyrrole for 5 min) and (c, d) CoFe LDH@PPy/CC-15 (electrochemical polymerization of pyrrole for 15 min) samples.
7. **Fig. S7** SEM images of (a, b) CoFe@NC/CC-5, (c, d) CoFe@NC/CC-15.
8. **Fig. S8** Raman spectra for a CoFe LDH/CC and CoFe@NC/CC.
9. **Fig. S9** Wide XPS spectra of (a) CoFe LDH/CC, (b) CoFe@NC/CC and (c) High-resolution XPS spectra of C1s for CoFe@NC/CC.
10. **Fig. S10** (a) OER LSV curves and (b) tafel plots of CoFe@NC-5/CC and CoFe@NC-15/CC. (c) ORR LSV curves and (d) tafel plots of CoFe@NC-5/CC and CoFe@NC-15/CC.
11. **Fig. S11** (a) OER LSV curves and (b) tafel plots of CoFe/CC. (c) ORR LSV curves and (d) tafel plots of CoFe/CC.
12. **Fig. S12** CV curves of (a) CoFe LDH/CC, (b) CoFe@NC-5/CC, (c) CoFe@NC/CC and (d) CoFe@NC-15/CC catalysts at different scan rates of 10~50mV s<sup>-1</sup> in the potential range of 1.04~1.25 V (vs. RHE).
13. **Fig. S13** The corresponding current density as a function of scan rate derived from Figure S12.
14. **Fig. S14** EIS Nyquist plots for all compared catalysts.
15. **Fig. S15** (a) OER LSV curves and (b) ORR LSV curve of CoFe-10@NC/CC, CoFe-20@NC/CC and CoFe-30@NC/CC.

16. **Fig. S16** (a) LSV curves at different electrode rotating speeds from 400 to 2500 rpm and the corresponding fitted K–L plots at different potentials for Pt/C catalysts. (b) Durability of Pt/C catalyst for ORR.
17. **Fig. S17** (a) Open circuit voltage of the battery assembled with CoFe@NC/CC as air-cathode. (b) Photograph of a light emitting diode (LED) illumed by three liquid ZABs in series.
18. **Fig. S18** Galvanostatic discharge–charge cycling profiles of CoFe drop coating catalyst at a current density of  $10\text{mA cm}^{-2}$ .
19. **Fig. S19** Galvanostatic discharge–charge profiles of CoFe@NC/CC-based battery at a current density of  $20\text{mA cm}^{-2}$  with a cycling interval of 40 min (20 min for charging and 20 min for discharging).
20. **Fig. S20** (a) XRD pattern, High-resolution XPS spectra of (b) Co 2p and (c) Fe 2p for CoFe@NC/CC after electrochemical test.
21. **Fig. S21** Open circuit voltage of the all-solid-state Zn-air batteries with CoFe@NC/CC as air-cathodes.
22. **Table S1.** ORR and OER performances for CoFe@NC/CC and all compared catalysts.
23. **Table S2.** The electrochemical impedance spectroscopy fitted results for all catalysts.
24. **Table S3.** The comparison of OER and ORR performance of CoFe@NC/CC with recently reported non-precious metal powdery catalyst.
25. **Table S4.** Zn-air batteries performances of CoFe@NC/CC, CoFe@NC+CC and Pt/C+RuO<sub>2</sub> catalysts.
26. **Table S5.** Summary of Zn-air battery performances of this work with recently reported results.

## Computational methods of density functional theory (DFT) calculations

Density functional theory (DFT) calculations were performed by using the CASTEP packages.<sup>S1</sup> The exchange-correlation energies were calculated according to the Perdew-Wang scheme within the general gradient approximation (PBE) framework.<sup>S2</sup> With the application of the ultrasoft potential (J. P. Perdew, K. Burke, M. Ernzerhof, phys. Rev. Lett., 1996, 77, 3865), the energy cutoff was 340 eV. The integration of Brillouin-zone was treated by a (4×4×1) grid, and a vacuum region (15 Å) was added above each slab to avoid the fake interaction along z axis. Stable configurations were obtained by a geometry optimization, and the iterations were repeated until the forces on the atoms were less than 0.03 eV/Å and the energy change less than 1.0×10<sup>-5</sup> eV. The adsorption energy ( $E_{ads}$ ) is defined as the following equation:

$$E_{ads} = E_{surf+O_2} - E_{surf} - E_{O_2}$$

$E_{surf+O_2}$  is the total energy of the O<sub>2</sub>/material system,  $E_{surf}$  is the material surface energy, and  $E_{O_2}$  is the free O<sub>2</sub> molecule.

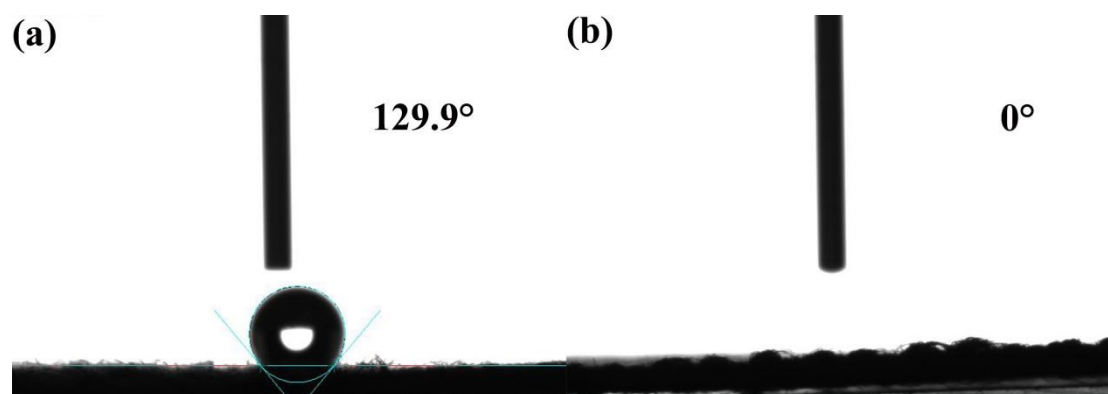


**Fig. S1** Contact angle photos of CC before (a) and after (b) oxidation treatment.

As the photos illustrated in **Fig. S1**, the contact angles for CC before and after oxidation treatment were about  $129.9^\circ$  and  $0^\circ$ , respectively. It was indicated that the CC changed from the original hydrophobicity to hydrophilicity, which could be beneficial to the contact between the electrolyte and the catalyst. Therefore, the oxidation treatment of CC was very significant.

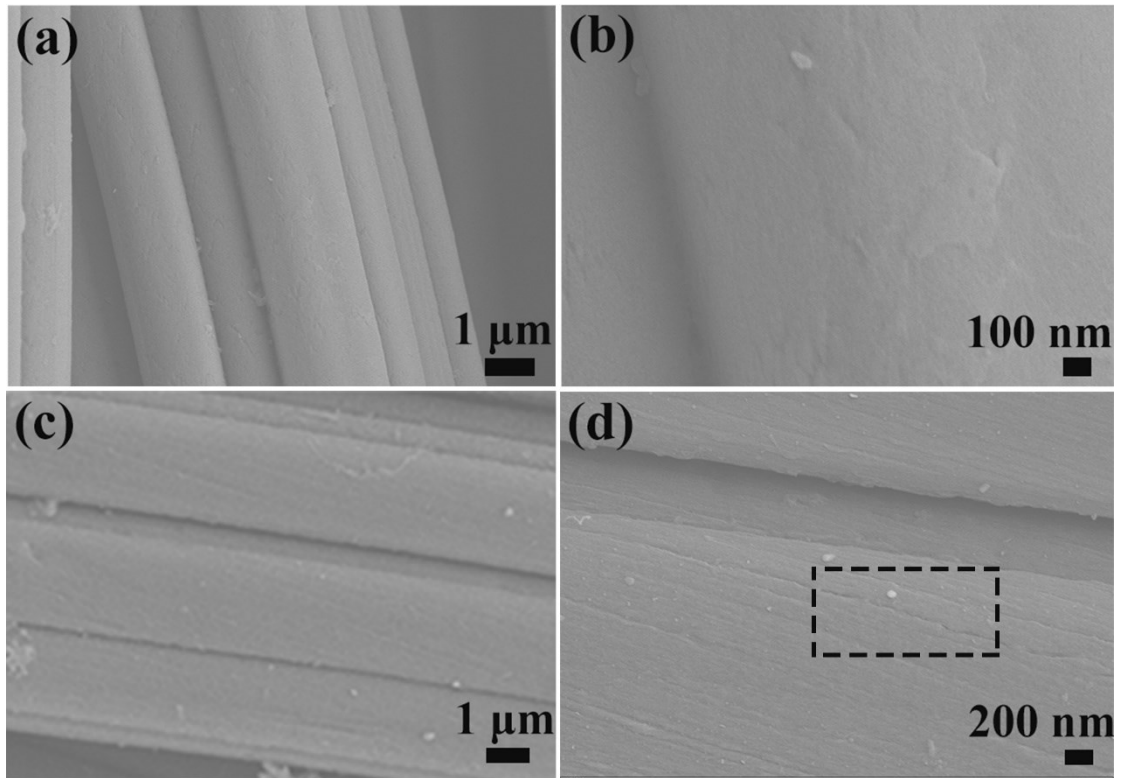


**Fig. S2** SEM images of CC before (a, b) and after (c, d) oxidation treatment.

As the SEM images shown in **Fig. S2**, the oxidation treated CC obviously exhibit the shallow grooves and wrinkles compared with the originated CC, which could increase the contact area of electrolyte and reactant. Moreover, the plentiful oxygen-containing functional group could enhance oxygen reaction activity.

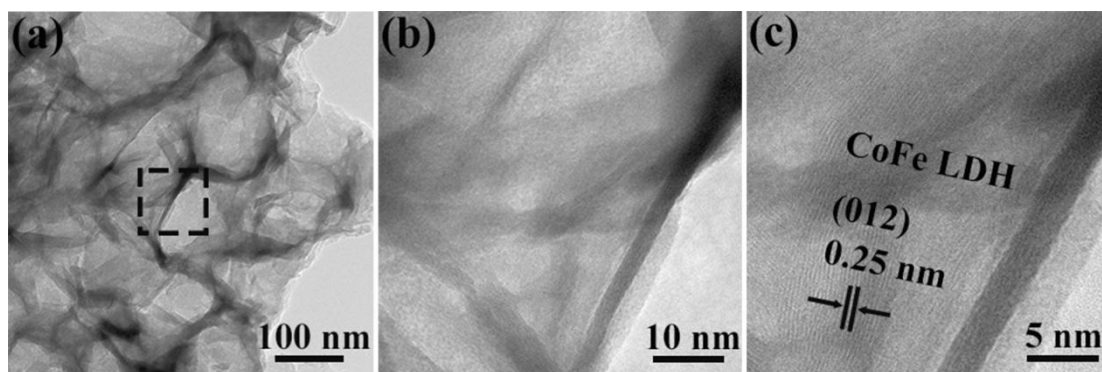


**Fig. S3** (a) TEM and (b,c) HRTEM images of CoFe LDH/CC sample.

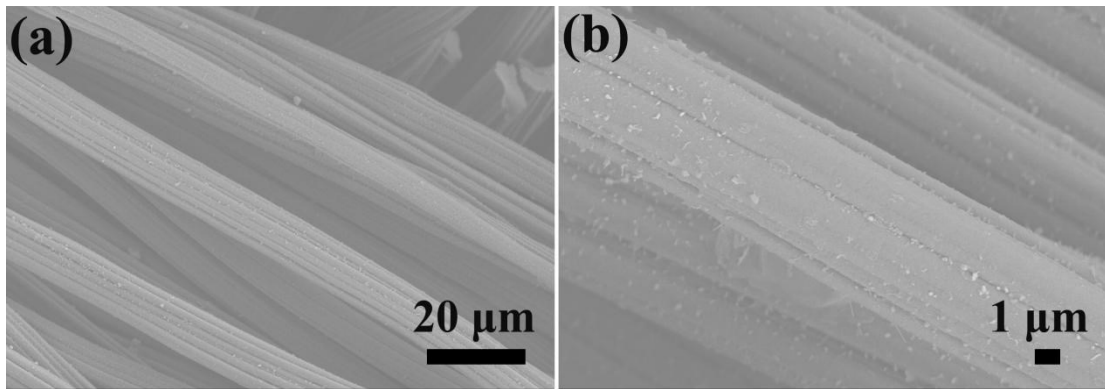


**Fig. S4** SEM images of CoFe LDH grown on carbon cloth without oxidation treatment.

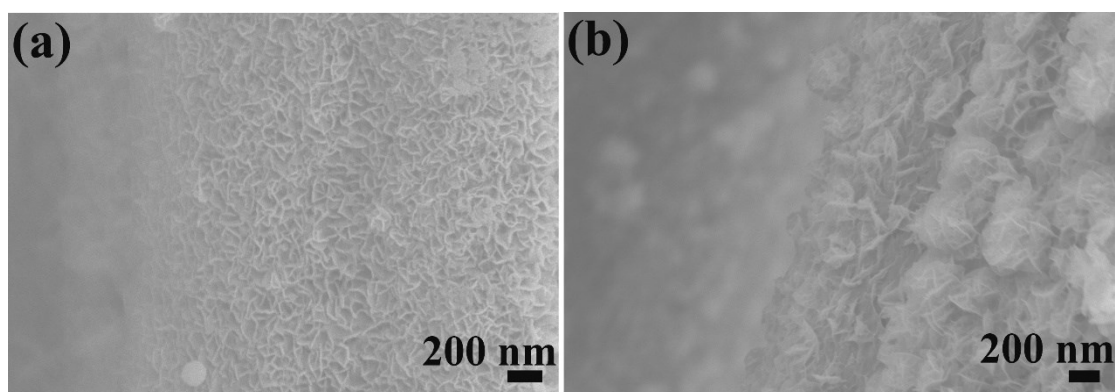


**Fig. S5** SEM images of (a) CoFe LDH-30 and (b) CoFe LDH-150 samples.

In contrast, the electrodeposition time of CoFe LDH grown on CC was changed to 30 s and 150 s were respectively prepared. As shown in **Fig. S5a**, the morphology of the sheet structure did not change greatly with when the electrodeposition time decreased to 30 s, but the low catalyst loading would affect the activity of the catalyst. If the electrodeposition time was extended to 150 s, a lot of CoFe nanosheets could assemble to nanoflower structures and stack on the surface of LDH nanosheets (**Fig. S5b**), which was not stable and could affect the mass transfer. Based on the above analyses, the 90 s electrodeposition time was the optimum reaction time in our synthesis.

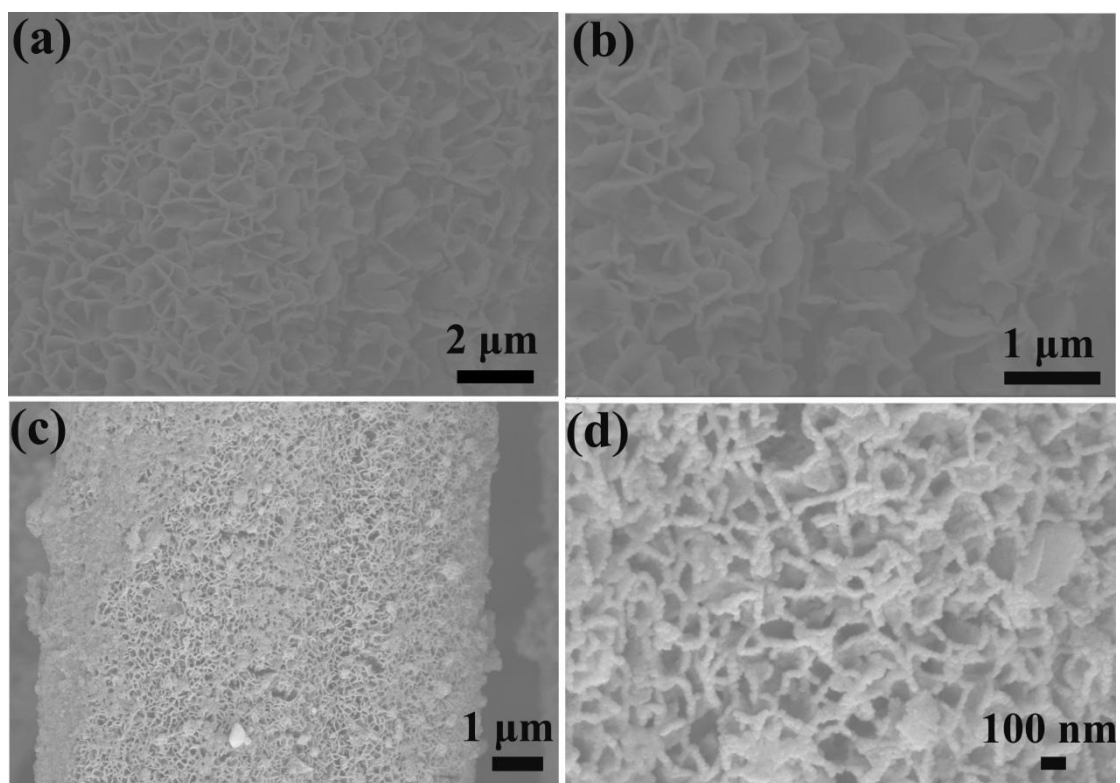


**Fig. S6.** SEM images of (a, b) CoFe LDH@PPy/CC-5 (electrochemical polymerization of pyrrole for 5 min) and (c, d) CoFe LDH@PPy/CC-15 (electrochemical polymerization of pyrrole for 15 min) samples.

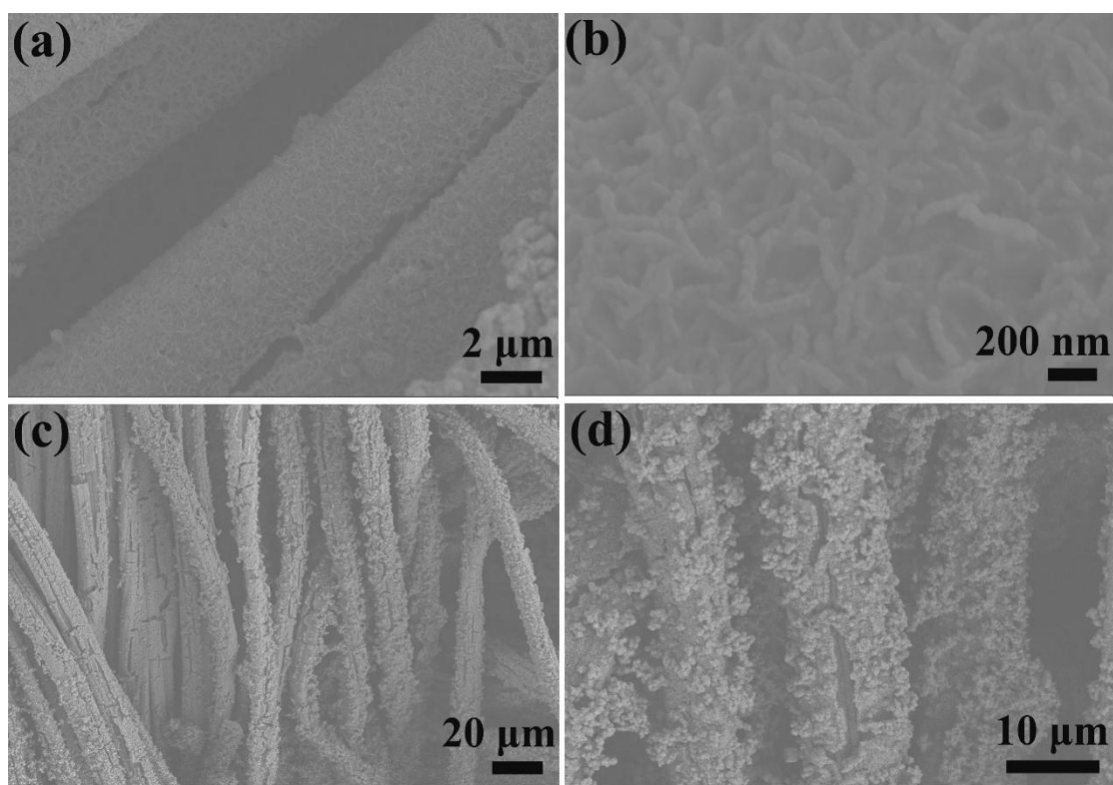


**Fig. S7** SEM images of (a, b) CoFe@NC/CC-5, (c, d) CoFe@NC/CC-15.

When the reaction time was decreased to 5 min, the thickness of nanosheets in the CoFe LDH/CC-5 sample could not be obviously changed compared with the CoFe LDH/CC (Fig. S6a, S6b). The corresponding pyrolyzed CoFe@NC/CC-5 sample exhibited wormlike coated surface (Fig. S7a, S7b). Because the obtained nanosheets derived from 5 min electrodeposition is relative thin, the CoFe@NC/CC-5 cannot well withstand after pyrolysis, resulting in the layer structure completely destroyed and a wormed structure formed. It sharply reduced the specific surface area and mass transfer channels. Moreover, the thickness of nanosheets in the CoFe LDH/CC-15 (electrochemical polymerization 15 min) sample apparently increased (Fig. S6c, S6d). After a pyrolysis treatment at 700 °C in nitrogen ambient, the CoFe@NC/CC-15 sample showed a cracked surface with severe nanoparticle aggregation due to the presence of large amounts of polypyrrole (Fig. S7c, S7d). It is indicated that the morphology and structures of CoFe@NC/CC can be controlled by adjusting the time for electrochemical polymerization of pyrrole.

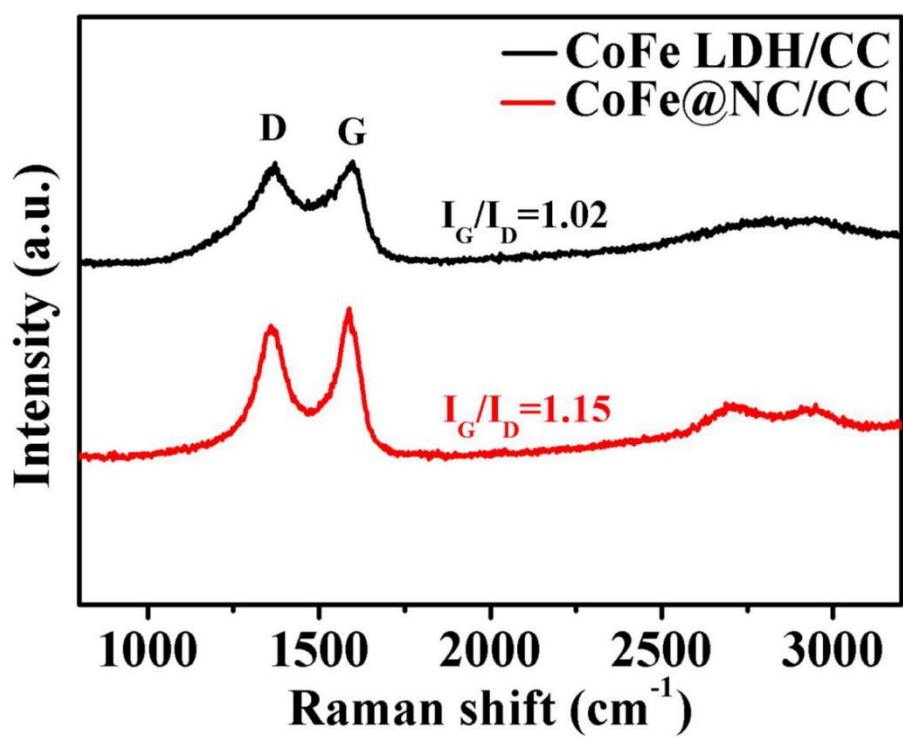
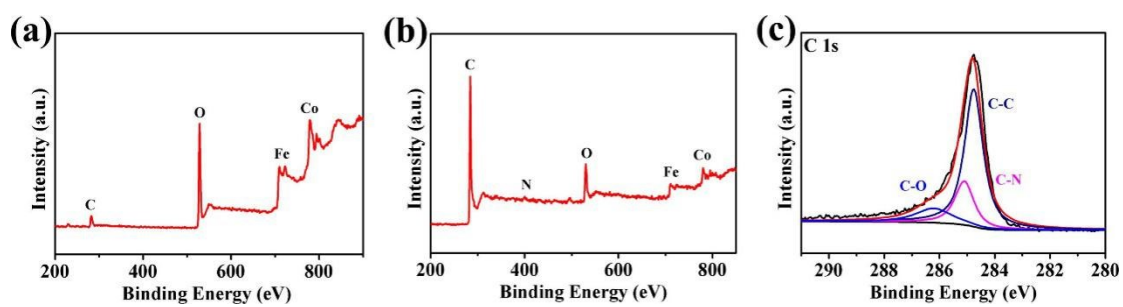
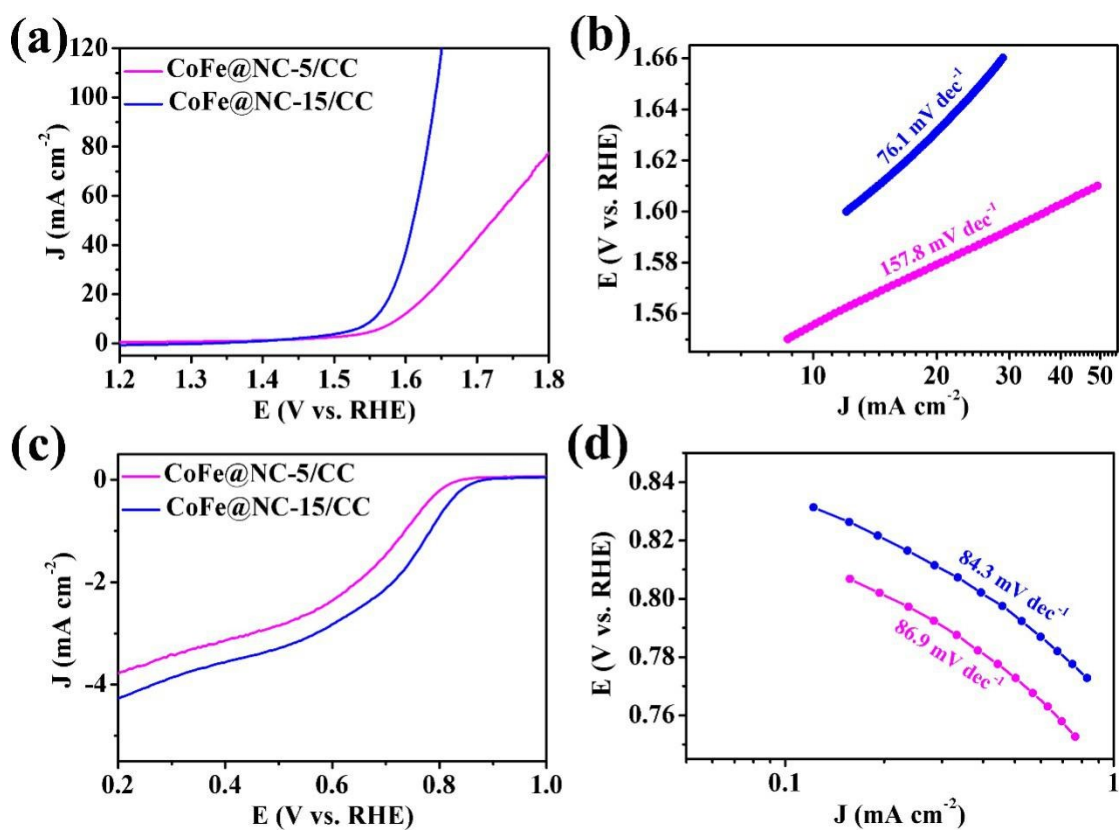


Fig. S8 Raman spectra for a CoFe LDH/CC and CoFe@NC/CC.



**Fig. S9** Wide XPS spectra of (a) CoFe LDH/CC, (b) CoFe@NC/CC and (c) High-resolution XPS spectra of C1s for CoFe@NC/CC.



**Fig. S10** (a) OER LSV curves and (b) tafel plots of CoFe@NC-5/CC and CoFe@NC-15/CC. (c) ORR LSV curves and (d) tafel plots of CoFe@NC-5/CC and CoFe@NC-15/CC.

**Table S1.** The ORR and OER performances for all compared catalysts.

Sample	$\eta_{10}$ for OER (V vs. RHE)	$\eta_{100}$ for OER (V vs. RHE)	$E_{\text{onset}}$ for ORR (V vs. RHE)	$E_{1/2}$ for ORR (V vs. RHE)
CoFe LDH/CC	1.54	1.69	0.86	0.69
<b>CoFe@NC/CC</b>	<b>1.48</b>	<b>1.54</b>	<b>0.92</b>	<b>0.75</b>
CoFe@NC+CC	1.66	1.76	0.83	0.63
CoFe@NC-5/CC	1.59	1.85	0.84	0.66
CoFe@NC-15/CC	1.56	1.64	0.89	0.70
RuO <sub>2</sub> /CC	1.59	2.07	NA	NA
Pt/C	NA	NA	0.99	0.83

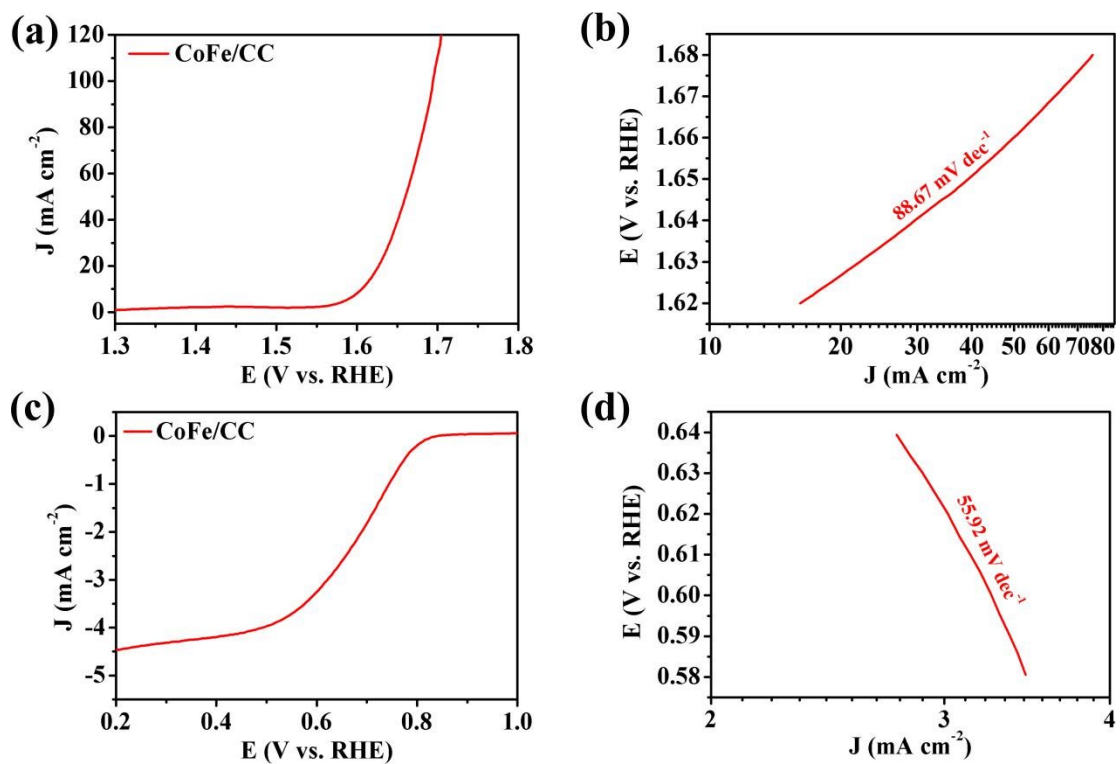


**Fig. S11** (a) OER LSV curves and (b) tafel plots of CoFe/CC. (c) ORR LSV curves and (d) tafel plots of CoFe/CC.

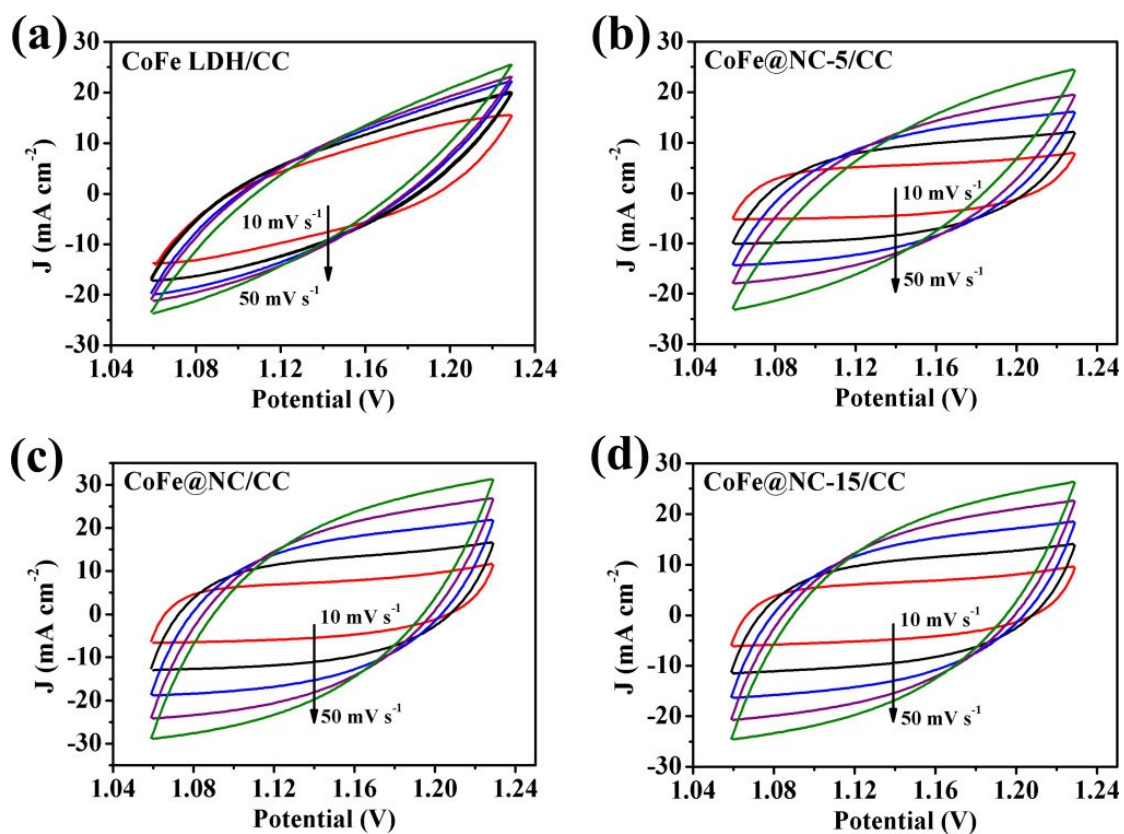


**Fig. S12** CV curves of (a) CoFe LDH/CC, (b) CoFe@NC-5/CC, (c) CoFe@NC/CC and (d) CoFe@NC-15/CC catalysts at different scan rates of 10~50mV s<sup>-1</sup> in the potential range of 1.04~1.25 V (vs. RHE).

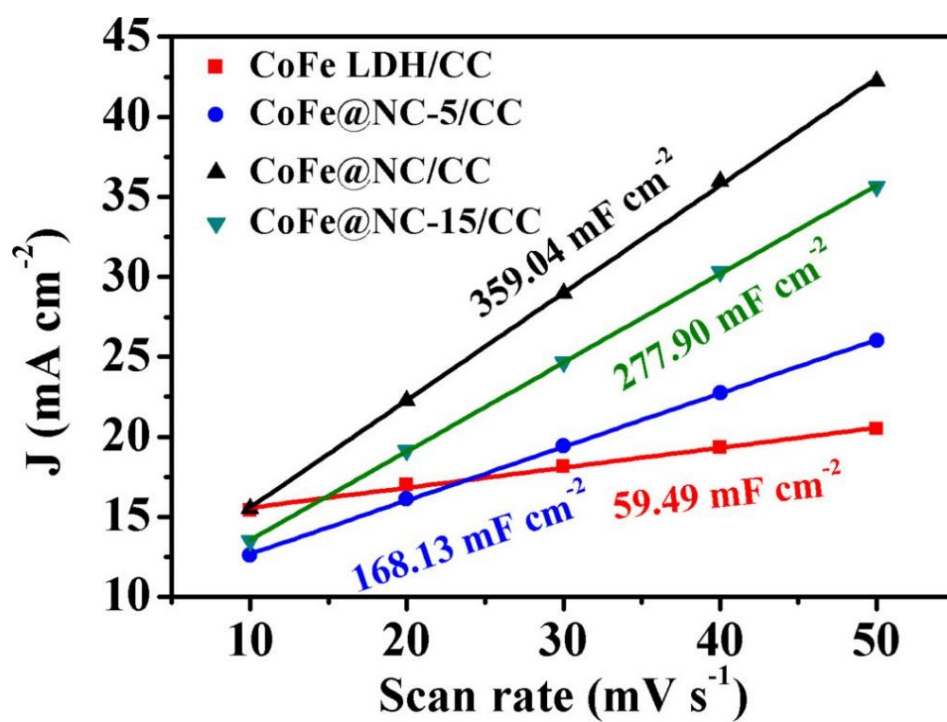


**Fig. S13** The corresponding current density as a function of scan rate derived from Fig. S12.

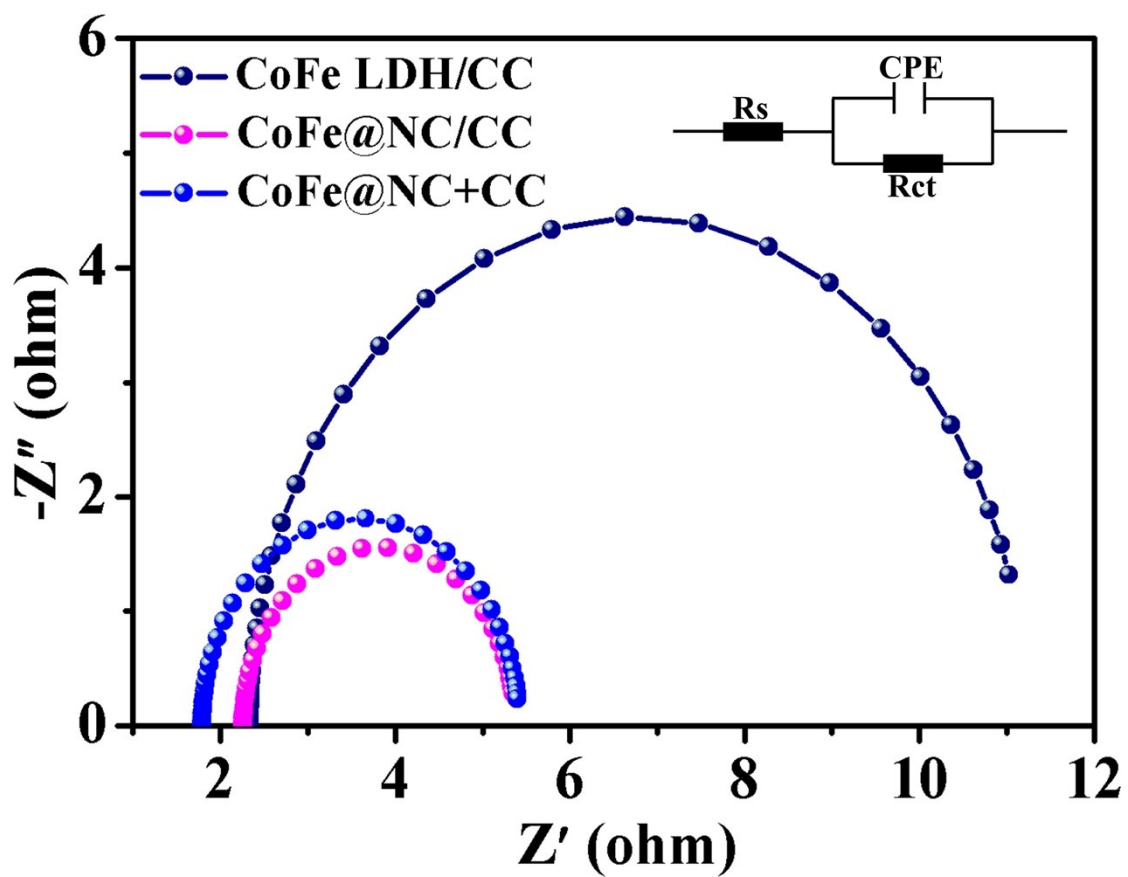
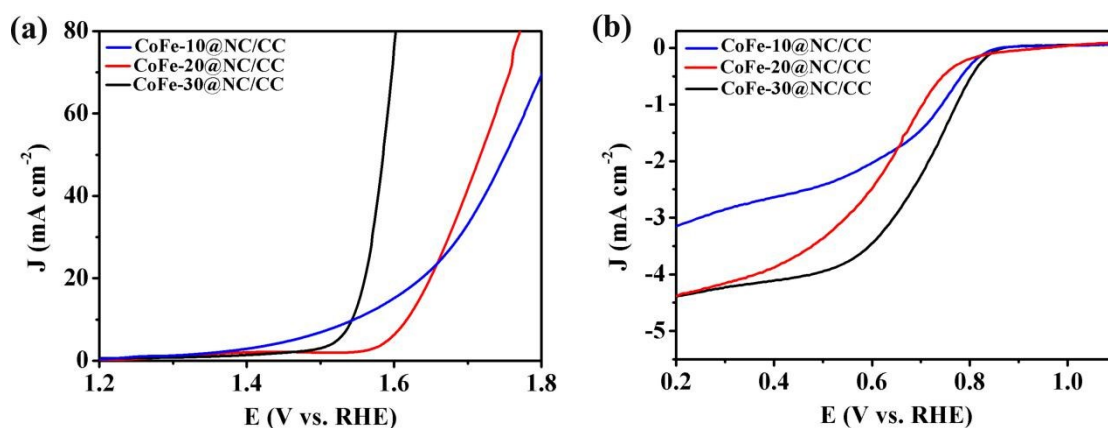


Fig. S14 EIS Nyquist plots for all compared catalysts.

**Table S2.** The electrochemical impedance spectroscopy fitted results for all catalysts.

Samples	$R_s(\Omega)$	$R_{ct}(\Omega)$
CoFeLDH/CC	2.01	13.06
<b>CoFe@NC/CC</b>	<b>0.23</b>	<b>3.11</b>
CoFe@NC+CC	1.50	4.33



**Fig. S15** (a) OER LSV curves and (b) ORR LSV curve of CoFe-10@NC/CC, CoFe-20@NC/CC and CoFe-30@NC/CC.

For comparison, we have supplemented the catalysts derived from the CoFe LDH electrodeposition time of 10s, 20s, and 30s, and the corresponding products were denoted as CoFe-10@NC/CC, CoFe-20@NC/CC and CoFe-30@NC/CC, respectively. As shown in Fig. S15, all the catalysts exhibited unideal OER and ORR performances owing to the low catalyst loading.

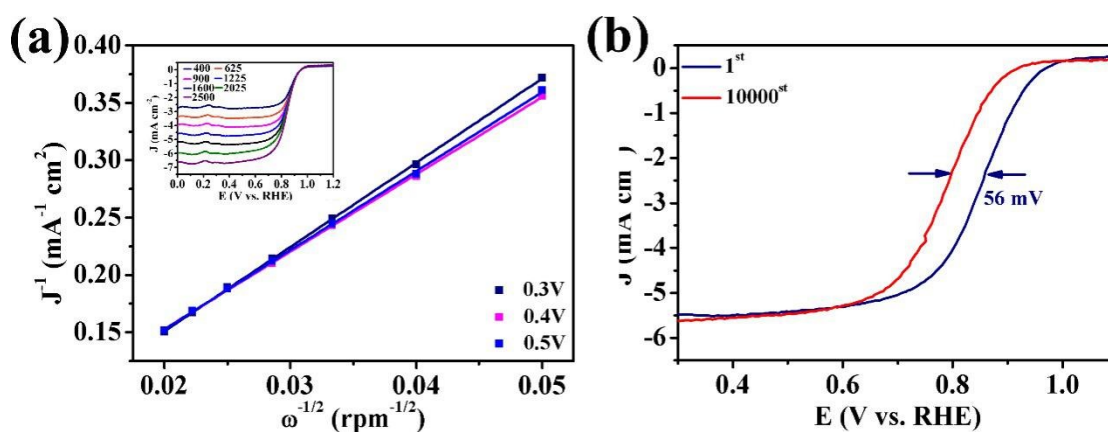


**Fig. S16** (a) LSV curves at different electrode rotating speeds from 400 to 2500 rpm and the corresponding fitted K–L plots at different potentials for Pt/C catalysts. (b) Durability of Pt/C catalyst for ORR.

**Table S3.** The comparison of OER and ORR performance of CoFe@NC/CC with recently reported non-precious metal powdery catalyst.

Sample	$\eta_{10}$ for OER (V vs. RHE)	$E_{\text{onset}}$ for ORR (V vs. RHE)	$E_{1/2}$ for ORR (V vs. RHE)	References
CoFe@NC/CC	1.48	0.92	0.75	This work
NiO/CoN PINWs	1.53	0.89	0.69	S3
Ni-Fe-MoN NTs	1.46	0.88	0.72	S4
CoFeS <sub>1.6</sub> (OH) <sub>1.8</sub>	1.59	0.88	0.72	S5
NCo-250	1.55	0.95	0.75	S6

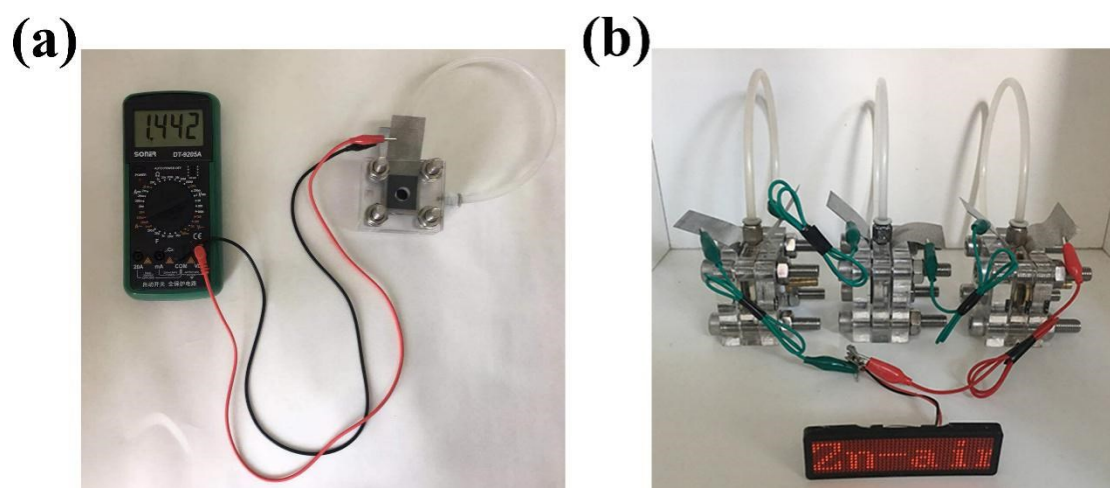


**Fig. S17** (a) Open circuit voltage of the battery assembled with CoFe@NC/CC as air-cathode. (b) Photograph of a light emitting diode (LED) illumed by three liquid ZABs in series.

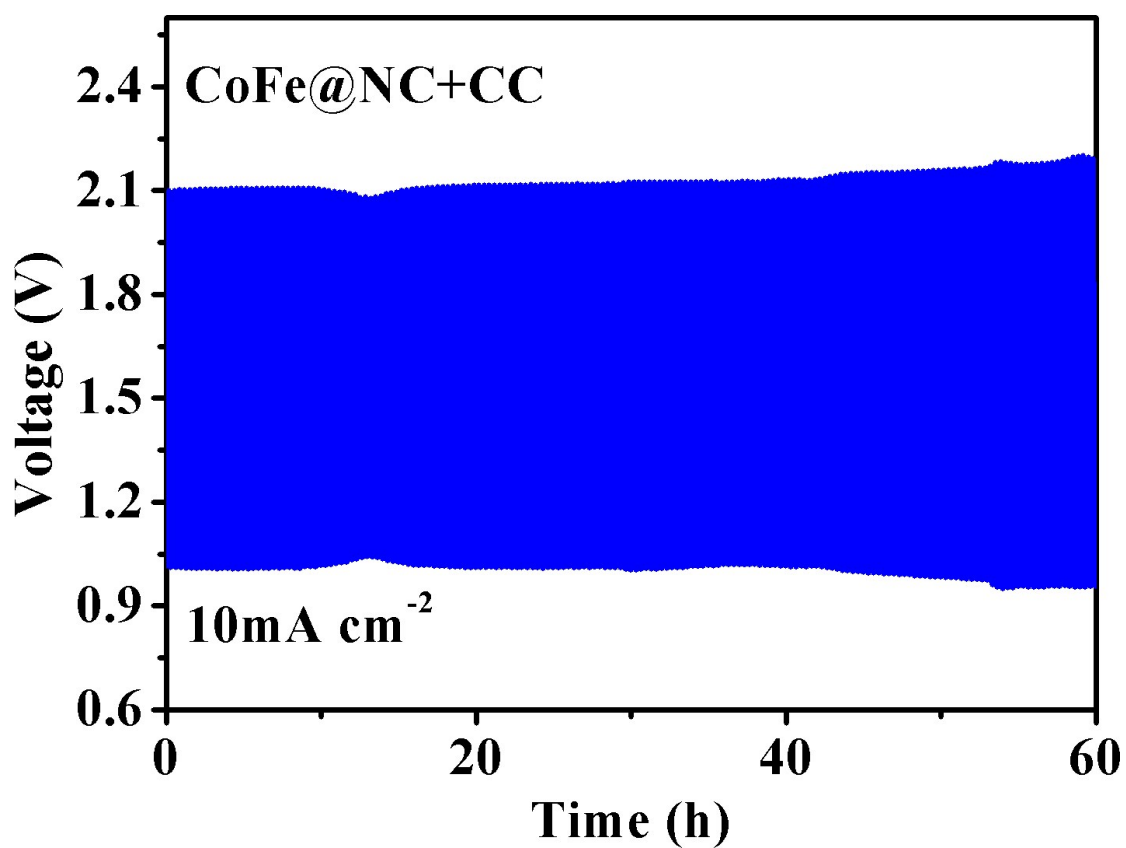


**Fig. S18** Galvanostatic discharge-charge cycling profiles of CoFe drop coating catalyst at a current density of  $10\text{mA cm}^{-2}$ .

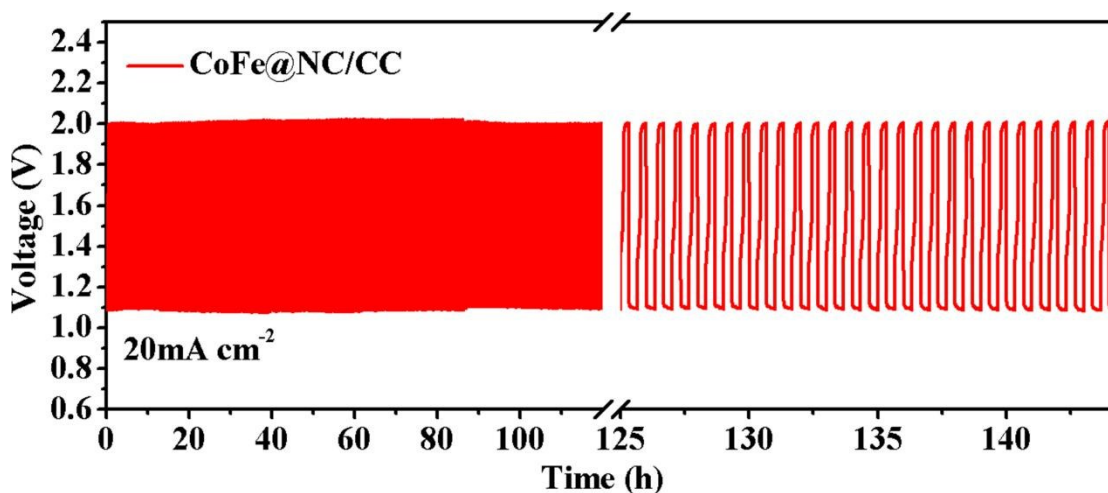


**Fig. S19** Galvanostatic discharge–charge profiles of CoFe@NC/CC-based battery at a current density of  $20\text{mA cm}^{-2}$  with a cycling interval of 40 min (20 min for charging and 20 min for discharging).

**Table S4.** Zn-air batteries performances of CoFe@NC/CC, CoFe@NC+CC and Pt/C+RuO<sub>2</sub> catalysts.

Sample	Initial voltage gap (V)	Final voltage gap (V)	Cycle time (h)
<b>CoFe@NC/CC</b>	<b>0.75</b>	<b>0.76</b>	<b>261</b>
CoFe@NC+CC	1.09	1.18	60
Pt/C+RuO <sub>2</sub>	0.96	1.71	41.2

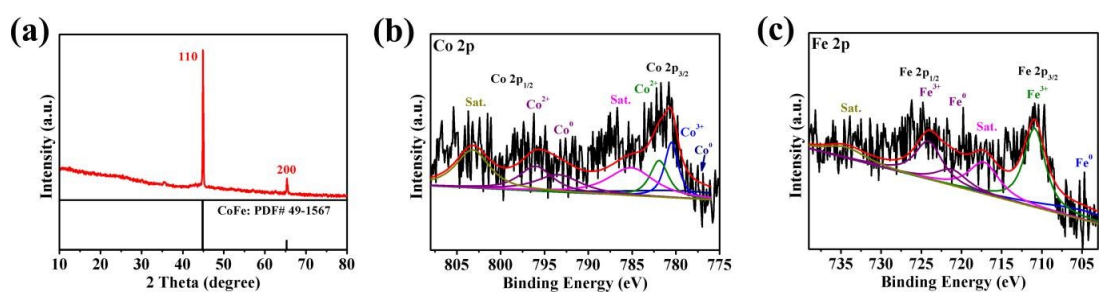


**Fig. S20** (a) XRD pattern, High-resolution XPS spectra of (b) Co 2p and (c) Fe 2p for CoFe@NC/CC after electrochemical test.



**Figure S21.** Open circuit voltage of the all-solid-state Zn-air batteries with CoFe@NC/CC as air-cathodes.

**Table S5.** Summary of Zn-air battery performances of this work with recently reported results.

Sample	Liquid ZAB			All-solid-state ZAB			References
	First	Final	Current	Cycling	Current	Cycling	
	charge/discharge	Charge/discharge	density	time	density	time	
	Voltage gap (V)	Voltage gap (V)	(mA cm <sup>-2</sup> )	(h)	(mA cm <sup>-2</sup> )	(h)	
Co-SAs@NC	0.81	0.85	10	85	1;2	17;12	S7
Fe-Co <sub>3</sub> O <sub>4</sub> /CC	0.75	0.77	2	100	-	-	S8
CuCoP-NC-700	0.75	0.75	10	80	-	-	S9
NiFe@N-CFs	0.66	0.77	10	233	1	10	S10
CoFe/SN-C-25	0.90	0.91	10	85	-	-	S11
Fe <sub>0.5</sub> Co <sub>0.5</sub> O <sub>x</sub> /NrGO	0.79	0.89	10	120	-	-	S12
CoS <sub>x</sub> /Co-NC-800	0.79	0.80	2	200	1	7	S13
Co <sub>3</sub> FeS <sub>1.5</sub> (OH) <sub>6</sub>	0.84	0.84	2	36	-	-	S14
FeN <sub>x</sub> /C-700-20	1.42	1.02	5	84	-	-	S15
Fe-Co <sub>4</sub> N@N-C	0.80	0.81	5	36	4	7.5	S16
<b>CoFe@NC/CC</b>	<b>0.75</b>	<b>0.76</b>	<b>10</b>	<b>261</b>	<b>2</b>	<b>16</b>	<b>This work</b>

### References in supporting information:

- S1.** S. J. Clark, M. D. Segall, C. J. Pickard, P. J. Hasnip, M. J. Probert, K. Refson and M. C. Payne, *Zeitschrift fuer Kristallographie.*, 2005, **220**, 567-570.
- S2.** J. Perdew and Y. Wang, *Phys. Rev. B.*, 1992, **45**, 13244-13249.
- S3.** J. Yin, Y. Li, F. Lv, Q. Fan, Y. Q. Zhao, Q. Zhang, W. Wang, F. Cheng, P. Xi and S. Guo, *ACS nano.*, 2017, **11**, 2275–2283.
- S4.** C. Zhu, Z. Yin, W. Lai, Y. Sun, L. Liu, X. Zhang, Y. Chen and S. L. Chou, *Adv. Mater.*, 2018, **32**, 1802327.
- S5.** H. F. Wang, C. Tang, B. Wang, B. Q. Li, and Q. Zhang, *Adv. Mater.*, 2017, **29**, 1702327.
- S6.** J. Zhao, Y. He, Z. Chen, X. Zheng, X. Han, D. Rao, C. Zhong, W. Hu and Y. Deng, *ACS Appl. Mater. Interfaces*, 2019, **11**, 4915–4921..
- S7.** X. Han, X. Ling, Y. Wang, T. Ma, C. Zhong, W. Hu and Y. Deng, *Angew. Chem. Int. Ed.*, 2019, **58**, 5359-5364.
- S8.** X. Liu, T. Tang, W. Jiang, Q. Zhang, L. Gu and J. Hu, *ChemComm.*, 2020, **56**, 5374-5377.
- S9.** H. Zhang, Z. Yang, X. Wang, S. Yan, T. Zhou, C. Zhang, S. G. Telfer and S. Liu, *Nanoscale*, 2019, **11**, 17484-17395.
- S10.** Y. Niu, X. Teng, S. Gong and Z. Chen, *J. Mater. Chem. A*, 2020, **8**, 13725-13734.
- S11.** C. Li, E. Zhou, Z. Yu, H. Liu and M. Xiong, *Appl. Catal., B*, 2020, **269**, 118771.
- S12.** L. Wei, E. Karahan, S. Zhai, H. Liu, X. Chen, Z. Zhou, Y. Lei, Z. Liu and Y. Chen, *Adv. Mater.* 2017, **29**, 1701410.
- S13.** Q. Lu, J. Yu, X. Zou, K. Liao, P. Tan, W. Zhou, M. Ni and Z. Shao, *Adv. Funct. Mater.*, 2019, **3**, 1904481.
- S14.** H. F. Wang, C. Tang, B. Wang, B. Q. Li and Q. Zhang, *Adv. Mater.*, 2017, **29**, 1702327.
- S15.** S. Han, X. Hu, J. Wang, X. Fang and Y. Zhu, *Adv. Energy Mater.*, 2018, **8**, 1800955.

**S16.** Q. Xu, H. Jiang, Y. Li, D. Liang, Y. Hu and C. Li, *Appl. Catal., B*, 2019, **256**, 117893.